

State of the Art of Gadolinium Zirconate Based Thermal Barrier Coatings: Design, Processing and Characterization

Mustafa Guven Gok and Gultekin Goller

Abstract

The fast consumption of fossil fuel resources and economic competitiveness makes it necessary to increase the efficiency of turbine engines. For this purpose, thermal barrier coating (TBC) has been used on some critical parts of gas turbines. Yttria-stabilized zirconia (YSZ) is widely and commercially used as a ceramic top coat material for TBC in the gas turbine system. On the other hand, the efforts to identify new material having better properties than YSZ have been continued. Gadolinium zirconate (GZ) is a promising alternative TBC material with its lower thermal conductivity, better sintering ability, and higher melting point and phase stability than YSZ. However, recent research studies on the responses of GZ-based TBC materials to the complex demands of modern gas turbine applications should be gathered under a study by comparing them with the results of traditional TBC material. This chapter discusses the GZ based TBC system, specifically addressing issues related to the production process and designing of the coating architecture, in comparison with some of the significant properties with YSZ and the test methodology. Moreover, the chapter also contains information about laser surface modification of the GZ-based TBC.

Keywords: thermal barrier coating, gadolinium zirconate, multilayered, functionally graded, thermal conductivity, thermal cycling, thermal shock, hot corrosion, CMAS resistance, laser surface modification

1. Introduction

Temperature acting on hot section of gas turbine goes up to about 1300°C during engine operation. However, metallic materials cannot be used at these temperatures due to harsh effect of the high temperature. Therefore, a thermal barrier coating (TBC) system is needed to satisfy effective protection to the metallic components of the gas turbine engines [1–3]. Generally, a conventional TBC system consists of four layers having different functions, as seen in **Figure 1**.

The first part of a TBC system is metallic substrate. Ni-based superalloys (INCONEL) are the most widely used metallic materials in parts of the turbine blade and combustion chamber due to their resistance to high-temperature conditions [4]. Therefore, the substrate material of the TBC system is generally INCONEL alloys.

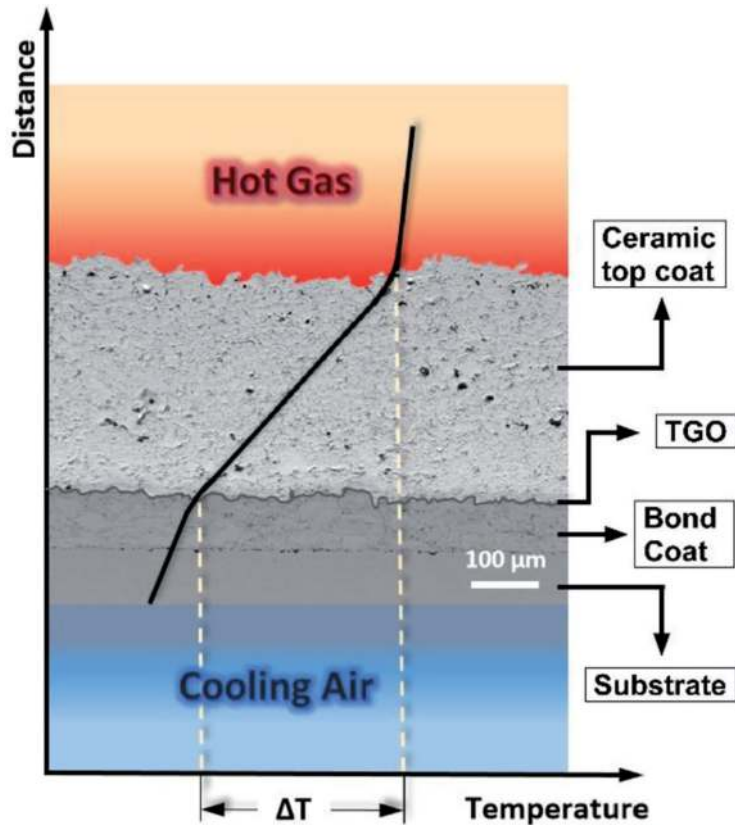


Figure 1.
Thermal barrier coating system.

The bond coat layer is the second part of the TBC system. The MCrAlY (M = Ni, Co, or both of them alongside Fe) bond coating powders are coated with a thickness of 75–150 μm on INCONEL substrate in different techniques such as high-velocity oxy-fuel (HVOF), atmospheric plasma spray (APS), suspension plasma spray (SPS), low-pressure or vacuum plasma spray (LPPS or VPS), and electron beam-physical vapor deposition (EB-PVD). HVOF is the most suitable method to produce the MCrAlY bond coating layer on the substrate due to its cheapness and sufficient characteristic properties [5]. The basic properties expected from the bond coating layer are as follows:

1. The bond coat should provide good oxidation resistance to metallic substrate.
2. The bond coat should provide good adherence between the metallic substrate and ceramic top coat.
3. The bond coat should tolerate the thermal expansion mismatch between the metallic substrate and ceramic top coat.

The third part of the TBC system is a thermally grown oxide (TGO, predominantly alpha-alumina) layer between the top coat and bond coat. A very thin TGO layer forms on the bond coat during coating process due to oxidation of the bond coat at the process temperatures, but it grows while the TBC system in gas turbine is operating at high temperatures. This layer has importance because failure of the TBCs mostly happens at the interface between TGO layer and ceramic top coat layer when the thickness of TGO layer reaches a critical value. At elevated temperatures

(>950°C), Al in the bond coat layer diffuses toward the bond coat layer/ceramic top coat layer interface. On the other hand, oxygen penetrates through the ceramic top coat layer and reacted with the Al. As a result, a TGO layer forms between the bond and the ceramic top coat [6–8].

The fourth and most important part of this system is ceramic top coat layer. Its principal role is to reduce the temperature of metallic substrate providing an insulation layer. Thus, efficiency of gas turbine engine is increased thanks to this thermal insulation layer, allowing higher turbine inlet temperatures (in the range of 100–300°C) and reduced cooling requirements. The thickness of the ceramic top coating layer ranges between 100 and 500 μm depending on the deposition method. Three different methods are used for the production of the ceramic top coat: (i) EB-PVD, (ii) APS, and (iii) SPS [1, 2, 7–14]. As seen in **Figure 2**, the main difference among these three methods is in the morphology of their microstructure.

APS coatings have a lamellar microstructure, while EB-PVD and SPS coatings have a columnar microstructure. Thus, ceramic top coating produced by APS technique has lower thermal conductivity due to microporosities between the lamellae. On the other hand, microporosities between the columns provide higher expansion tolerances in the ceramic top coating produced by EB-PVD and SPS techniques. The APS and SPS processes are more suitable for coating large parts and cheaper than EB-PVD process [10]. Static and stationary parts of the gas turbines are coated with a ceramic insulating material using APS process. A ceramic top coating layer suffers from the severe environmental effects of high temperature such as oxidation, hot

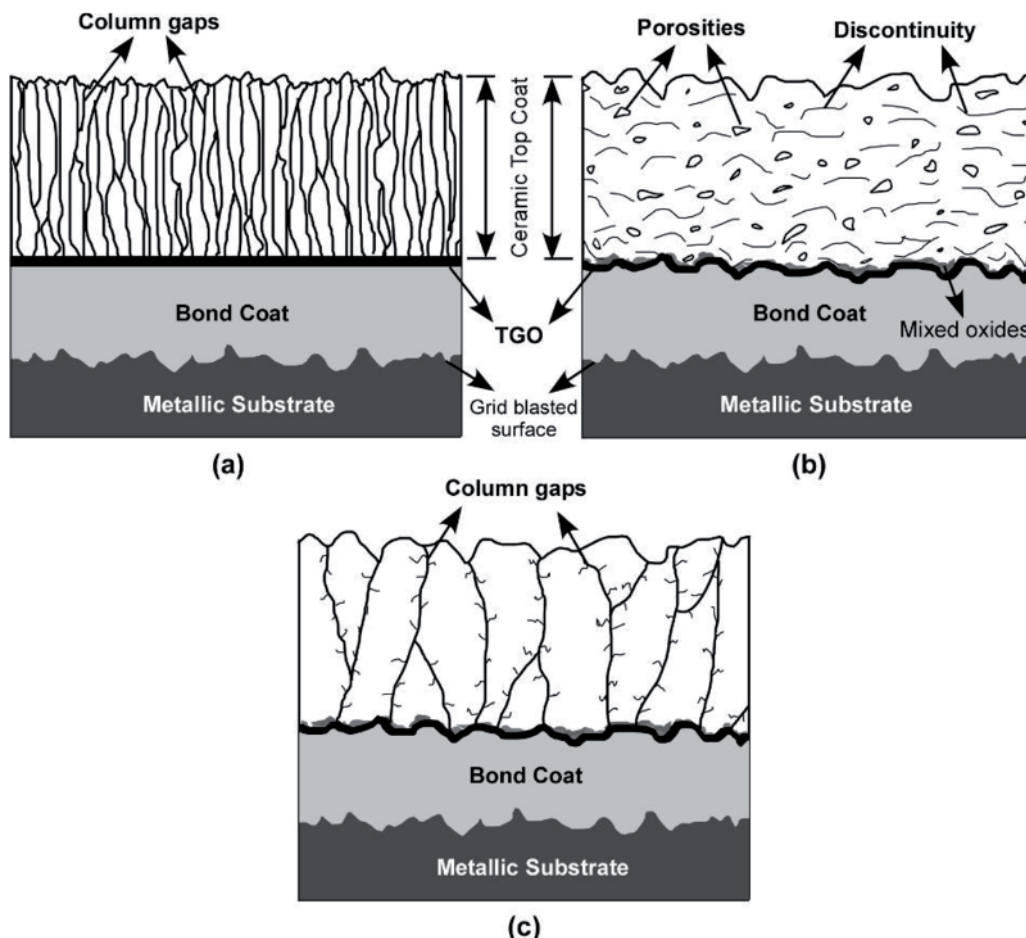


Figure 2. Schematic general structures of TBC produced by (a) EB-PVD method, (b) APS method, and (c) SPS method.

corrosion, wear, and flying ash damage. Therefore, a ceramic top coating material should have some important characteristic properties [15–17]. The basic properties expected from the ceramic top coating material can be listed as follows:

1. A ceramic top coating material should have high melting temperature to resist to the high temperature of gas plasma.
2. A ceramic top coating material should have low thermal conductivity to provide good insulation to the metallic substrate.
3. A ceramic top coating material should have high thermal expansion coefficient to match with the metallic bond coat and substrate's thermal expansion coefficient.
4. Phase structure of a ceramic top coating material should stay stable from room temperature to operating temperature.
5. A ceramic top coating material should adhere well to the metallic substrate.
6. A ceramic top coating material should have low sintering rate.
7. A ceramic top coating material should have high resistance to erosion, corrosion, and oxidation.

So far, no single coating material has been found which can fully meet all these properties listed above. However, it is believed that the best material that partially meets these properties is 6–8 wt% yttria-stabilized zirconia (YSZ) for more than 35 years now. Therefore, YSZ is widely and commercially used as a ceramic top coat for TBC in the gas turbine system at the present time. Although an alternative material has not yet been developed for YSZ, studies continue. These studies are important because YSZ has some undesirable properties, limiting working conditions of gas turbine listed below:

1. Above 1200°C, a diffusionless phase transformation from metastable tetragonal (t')-phase to tetragonal (t) and cubic (c) phase occurs above that temperature. This tetragonal phase transforms into monoclinic phase with a high volume change during cooling, and this phenomenon causes severe damages in the coating.
2. The porosity of the coating decreases due to sintering occurring above 1200°C, and thermally induced stresses come into existence. Failure possibility increases on the YSZ-based TBC due to these stresses.
3. YSZ has a high concentration of oxygen ion vacancies. Above 1200°C, these ion vacancies promote to oxygen transportation. Hence, a TGO layer forms between the bond coat and the ceramic top coat. When the thickness of this TGO layer reaches a critical value, spallation takes place in the ceramic top coating layer.
4. YSZ can be easily and seriously damaged from the hot corrosion induced by the existence of $\text{Na}_2\text{SO}_4 + \text{V}_2\text{O}_5$ salts coming from low-quality jet fuel and Ca-Mg-Al-silicate (CMAS) attack caused by flying ash. Both of them give rise to deterioration and spallation of the coating.

As a result of these undesirable properties:

1. The maximum use temperature use of YSZ is limited to below 1200°C.
2. YSZ is vulnerable to the hot corrosion and CMAS attack.

However, the TBC material of advanced next-generation powerful gas turbine engines must be able to operate without any damage both in harsh environments (under hot corrosion and CMAS attack) and at temperatures above 1200°C. The increase in efficiency in turbine engines is directly proportional to the increase in engine power and turbine inlet temperature. Therefore, an alternative ceramic top coat material having much better thermal properties than YSZ should be developed to be able to produce next-generation turbine engines. However, it is not easy to find a new material that will be an alternative to the YSZ [8, 13, 14, 18–21] because it requires a lot of experimental study, data, and evaluation.

Gadolinium zirconate ($\text{Gd}_2\text{Zr}_2\text{O}_7$ or GZ) with pyrochlore or defect fluorite-type structure is a new and promising alternative ceramic top coating material to YSZ. The most important features that make it advantageous are given below:

1. GZ has higher thermal stability at elevated temperatures (>1200°C) than YSZ. Therefore, it can be used at temperatures above 1200°C.
2. GZ has lower thermal conductivity (1.3 W/mK^{-1} at 1100°C) than YSZ (1.8 W/mK^{-1} at 1100°C). Thus, GZ provides better thermal insulation to the metallic substrate than YSZ.
3. GZ has more superior hot corrosion resistance than YSZ. Thanks to this feature, elements emitted due to fuel pollution are less harmful to the GZ-based TBC.
4. GZ has more resistance to the CMAS attack than YSZ. Because the CMAS powders (particles such as dust, volcanic ash, rock, etc.) entering to turbine melt at about 900 °C and try to penetrate through the coating surface. Porosities of the TBC are filled with CMAS, and thus strain incompatibility of the TBC is limited. This molten CMAS cannot penetrate to GZ-based TBC due to the sealing layer formed on the surface of the GZ-based TBC.

Thanks to these advantageous features, GZ seems to be the most efficient alternative TBC material for advanced next-generation powerful gas turbine engines. However, besides all of these advantages, GZ has two poor properties affecting its thermal cycling (TC) behavior in a negative manner. One of them is its low coefficient of thermal expansion (CTE, $10.4 \times 10^{-6} \text{ K}^{-1}$ and $11 \times 10^{-6} \text{ K}^{-1}$ for GZ and YSZ, respectively), and another one is its high tendency to react with the TGO layer [8, 9, 13, 14, 19, 21–32]. These problems were solved by using multilayered (MLed) and functionally graded (FGed) designs. In these MLed and FGed systems, a second material balances the poor properties (i.e., CTE) of other materials and improves TC performance of TBCs. On the other hand, the reaction between coating layer and TGO which fails the TC performance of rare earth zirconate will be prevented owing to a third layer between GZ and TGO layers [8, 13, 14].

The purpose of this chapter is to summarize the properties of GZ-based thermal barrier coatings. Their production techniques, coating designs, thermal conductivities, thermal cycling behaviors, mechanical properties, hot corrosion and CMAS resistance, and laser surface modification process were compiled in the following sections to form a meaningful whole.

2. Coating process and coating architectures

2.1 Production of gadolinium zirconate-based thermal barrier coatings

The performance and many properties of the TBC mainly depend on the microstructure and hence the production techniques. In literature, gadolinium zirconate-based thermal barrier coatings have been produced by different techniques such as the air plasma spraying (APS) [8, 13, 14], suspension plasma spraying (SPS) [25, 30], and electron beam-physical vapor deposition (EB-PVD) [20, 33].

In a study, GZ-based TBC was produced as single layered on metallic bond coat using the APS process [13]. The surface and cross-sectional microstructure of plasma-sprayed GZ-based TBC were shown in **Figure 3**. The surface roughness (R_a) was $8.3\ \mu\text{m}$, and typical surface properties (such as unmelted particles and open porosities) of APSed TBCs could be seen in **Figure 3a**. The micrographs demonstrate typical characteristic microstructure defects of APSed thermal barrier coatings such as cracks, both parallel (at splats boundaries) and normal to the metal/ceramic interface, and porosities. The interface between ceramic top coat/bond coats seems continuous and durable.

As seen in **Figure 4**, XRD patterns of GZ powder having an as-sprayed GZ-based coating proved that there was no decomposition after plasma spraying [8]. Both patterns had a cubic fluorite-type structure of GZ with the space group of $Fm\bar{3}m$. $\text{Gd}_2\text{Zr}_2\text{O}_7$ phase was maintained its stable position after APS process. Carpio et al. [23] showed that YSZ- and GZ-based TBCs had the same porosity value when

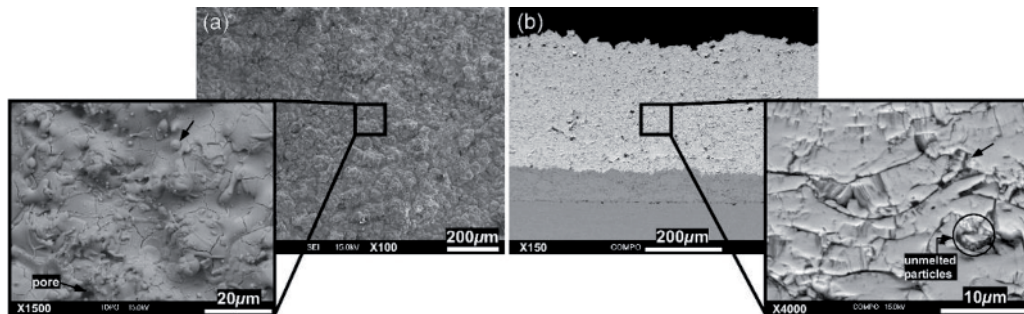


Figure 3. (a) Surface and (b) cross-sectional SEM images of atmospheric plasma-sprayed GZ coating.

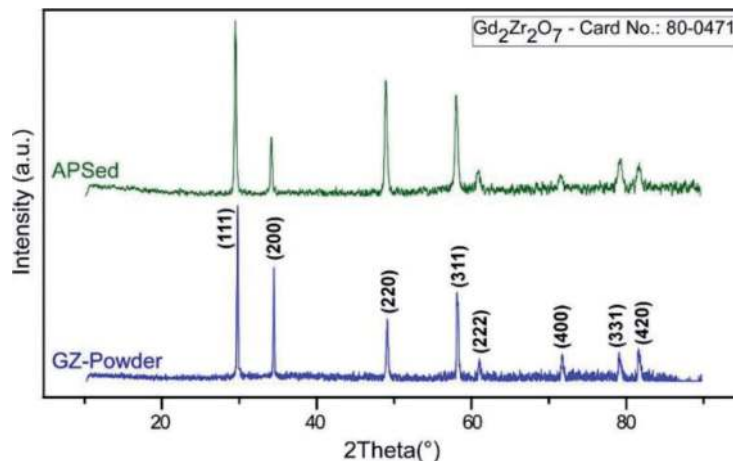


Figure 4. The XRD patterns of powder and atmospheric plasma-sprayed GZ coating.

the same APS parameters were used. These results indicate that there is no micro-structural problem in producing GZ by APS.

In different studies [25, 30], GZ-based TBCs were successfully produced on YSZ by suspension plasma spraying (SPS) process. SPSed GZ-based TBCs had nonporous and crack-free interface between the different top coat layers. In addition, SPSed GZ-based TBCs had a columnar microstructure having orientation perpendicular to the top surface which is a characteristic of the process. On the other hand, it is possible to obtain denser coating morphology by increasing droplet size via changing SPS parameters. Bozbin et al. [33] produced TBCs having GZ-based ceramic top coat by EB-PVD technique. The morphology of TBCs was columnar. This morphology was a characteristic of the coating produced by EB-PVD process. They showed that morphology of the GZ-based TBCs could be controlled by deposition process and temperature. The results of these studies [8, 13, 14, 20, 25, 30, 33] proved that GZ is a suitable material to be coated with different TBC production processes (such as APS, SPS, and EB-PVD).

2.2 Design of gadolinium zirconate-based thermal barrier coatings

Despite all the superior thermophysical properties of the single-layered GZ-based TBC, its thermal cycling lifetime is poor. Multilayered (as seen in **Figure 5a–c**) and functionally graded (as seen in **Figure 5d** and **e**) coating designs with a second TBC material have been used to overcome this problem [16]. In the multilayered (MLed) TBCs, there are two or more coating layers having different functions. On the other hand, a functionally graded (FGed) coating has gradual compositional variation in the layers. In these systems, a second material having higher coefficient of thermal expansion (CTE) balances the CTE of the system and improves TC performance of TBCs. The residual stress on the MLed and FGed coatings is lower than that of single-layered GZ [8, 14, 34]. The reaction between coating layer and TGO has been prevented owing to a second material adjacent to the top of the bond coat [8, 14].

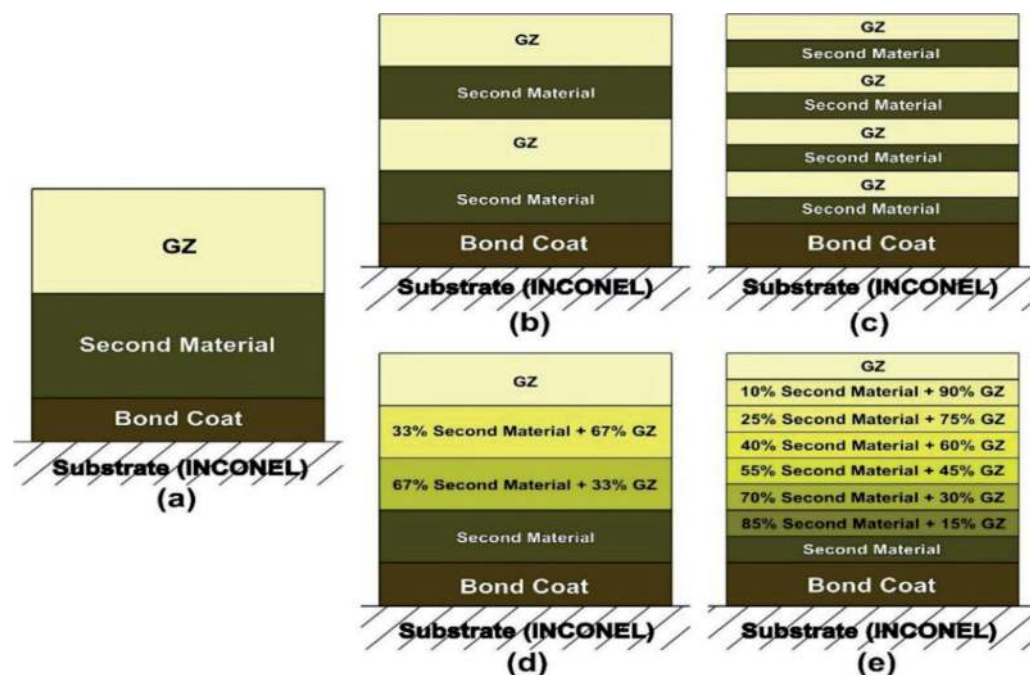


Figure 5. Schematic view of multilayered (a–c) and functionally graded (d, e) coating designs.

In a previous study [8], MLed and FGED gadolinium zirconate-based TBCs were produced in 2, 4, 8, and 12 layered by APS process. In this study, CYSZ was used as the second material because its CTE ($13 \times 10^{-6} \text{ K}^{-1}$) was better than that of GZ ($10.4 \times 10^{-6} \text{ K}^{-1}$). While producing a MLed system, CYSZ or GZ was sprayed to each layer. On the other hand, GZ and CYSZ powders were mixed at different ratios in a turbula-type mixer to obtain different compositions, and these mixtures of powders were sprayed to each layer. The average thickness of the ceramic top coat was $350 \mu\text{m}$. The interfaces between CYSZ and GZ layers were distinguishable, but there were no distinguishable interfaces between the different layers of FGED coatings. The following results were obtained from this study:

1. GZ and CYSZ powders sufficiently melted in the plasma flame.
2. Coating layers had characteristic microstructural defects of APSed TBCs.
3. Good lamination was achieved between GZ and CYSZ layers.
4. Porosity level of the ceramic top coating increased with the increasing number of layers.

The increase in the porosity level was explained by discontinuous coating process of MLed and FGED designs (layer-by-layer spraying).

In a study, double-layered and functionally graded GZ/YSZ coatings having five layers were produced with the thickness of $\sim 200 \mu\text{m}$ by APS process [23]. In the functionally graded GZ/YSZ TBC, ratio of the GZ to YSZ was different in each layer but bottom and top most layer were 100% YSZ and GZ, respectively. Researchers used two independent feeders to feed GZ and YSZ powders to the plasma flame, separately. Thus, there was no need to mix the powders before the APS process. Thanks to this system, different compositions could be obtained in each layer at the desired grade. It could be understood that it was possible to deposit the GZ and YSZ with functionally graded design by APS.

Mahade et al. [9, 29, 30] produced a double-layered GZ/YSZ and a triple-layered GZ dense/GZ/YSZ TBC by SPS process. The schematic view of their design was given in **Figure 6**. The morphology of the coatings was columnar, which was characteristic of the SPS, but dense in the topmost layer of the triple system. They aimed to increase the CMAS resistance of TBC thanks to a dense GZ layer on the topmost layer of triple-layered system. The density of coating layer was adjusted by changing the SPS parameters such as temperature and gas flow. The microstructure

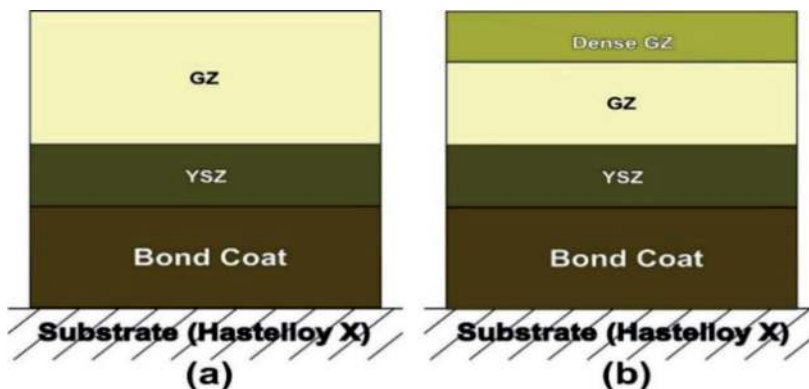


Figure 6. Schematic view of GZ/YSZ (a) double-layered and (b) triple-layered systems [9, 29, 30].

from the top surface of double-layered GZ/YSZ TBC was resembling a cauliflower, but top surface morphology of triple-layered TBC was denser due to dense GZ layer.

Multilayered GZ/YSZ TBCs having ten layers were deposited by EB-PVD process [35]. In addition, nano-layered GZ/YSZ TBCs having ~200 nm layer thickness were produced by the same process. The production of multilayered TBCs was carried out by alternating layers of GZ and YSZ during deposition. As expected, the morphology of the coating was columnar. These results proved that GZ-based TBCs could be deposited with different techniques and designs to improve some of their properties by using a second coating material.

3. Thermal properties

3.1 Thermal conductivity of gadolinium zirconate-based thermal barrier coatings

It can be said that the thermal conductivity is the most important property of the TBC. Therefore, mechanisms of heat transfer of the TBC material have a great significance. The phonons are primarily responsible for thermal conduction of ceramic materials. So thermal resistivity of the ceramic materials depends on the scattering of phonons. There are a lot of ways to scattering of phonons. One of them is to disturb the lattice vibration with additional scattering centers such as crystallographically changing to a lower symmetry, presence of different atoms inside a unit cell, porosities, grain boundaries, and impurities. As the number of these scattering centers increases, the thermal conductivity decreases [16]. Therefore, $Gd_2Zr_2O_7$ having pyrochlore and disordered fluorite structure has low thermal conductivity due to the oxygen vacancies in the unit cell.

Table 1 summarizes the lowest and highest thermal conductivity values of the GZ- and YSZ-based TBCs at specific temperature ranges produced by different techniques and having different coating designs. In addition, the thermal conductivity data of YSZ-based TBCs were given in **Table 1**. As understood from the data in the table, the thermal conductivity of the coating was influenced by the production method. This difference is entirely related to the different characteristics of microstructural morphology of the production processes. The lowest thermal conductivity values were obtained in the TBCs produced by APS due to its porous and lamellar morphology containing a lot of defects such as unmelted particles and cracks at splat boundaries. They acted as phonon scattering centers. On the other hand, thermal conductivity values of the TBCs produced by SPS and EB-PVD technique were higher than the TBCs produced by APS. This was because columnar morphology of the TBCs is produced by SPS and EB-PVD. Moreover, it is seen that the GZ-based TBCs had lower thermal than the YSZ-based TBCs produced by the same method and having the same design. This situation could be explained by oxygen vacancies acting as phonon scattering centers in the unit cell of GZ-based TBCs.

MLED and FGed GZ/CYSZ TBCs consisting 2, 4, 8, and 12 layers were produced by APS technique, and their thermal conductivity was analyzed by laser flash method [8]. Thermal conductivity values of the single-layered GZ and MLED and FGed GZ/CYSZ TBCs were lower than single-layered YSZ TBC ($0.91\text{--}1.79\text{ W/mK}^{-1}$ at $25\text{--}1105^\circ\text{C}$). Results showed that the lowest thermal conductivity values at 1105°C were achieved for ML12 and FG12 coatings having the highest number of layers. From this point of view, it was concluded that thermal conductivity value decreased by increasing the number of layers. This situation was attributed to the interfaces of the layered periodicity and increasing porosity level by increasing number of layers. Because these porosities and interfaces between GZ and CYSZ phases in the MLED

Design	Composition	Production technique	Thermal conductivity (W/mK ⁻¹)	Temperature (°C)	Reference
Single layered	GZ	APS	0.81–1.36	25–1105	[8]
Multilayered	GZ/CYSZ		0.63–1.76		
Functionally graded			0.56–1.55		
Single layered	GZ	APS	0.59–1.50	25–1100	[31]
Single layered	GZ	SPS	0.62–1.07	25–1000	[29]
Multilayered	GZ/YSZ		0.69–1.19		
Multilayered	GZ dense/GZ/YSZ		0.74–1.42		
Multilayered	GZ/YSZ	SPS	0.70–0.90	25–1200	[30]
Multilayered	GZ dense/GZ/YSZ		0.82–1.24		
Single layered	GZ	EB-PVD	1.10–2.10	400–1300	[33]
Multilayered	GZ/YSZ		1.60–2.10		
Single layered	GZ	EB-PVD	1.13–1.42	25–1316	[35]
Multilayered	GZ/YSZ + Yb ₂ O ₃ + Gd ₂ O ₃		1.10–1.22		
Fully dense	GZ	Sintering	1.47–1.83	25–1400	[28]
Fully dense	GZ	Sintering	1.65–2.05	200–1000	[3]
Fully dense	GZ	Sintering	1.60	700	[17]
Single layered	YSZ	APS	0.91–1.79	25–1105	[8]
Single layered	YSZ	SPS	1.57–1.96	25–1000	[29]
Single layered	YSZ	EB-PVD	1.38–1.62	400–1300	[33]
Fully dense	YSZ	Sintering	2.3	700	[17]

Table 1. Thermal conductivity of GZ- and YSZ-based materials produced via different processes and having different designs.

and FGeD designs acted as phonon scattering centers and reduced phonon conduction. Moreover, hemispherical reflection, that is, reduced phonon conduction, was thought to be active in the MLeD and FGeD designs. A similar phenomenon regarding the increasing hemispherical reflection by increasing the number of layers was reported in other studies [36].

Moskal et al. [31] produced single-layered GZ and YSZ TBCs by APS processes and compared their thermal conductivity at the temperatures between 25 and 1100°C. According to the results, GZ-based TBC had lower thermal conductivity (0.59–1.50 W/mK⁻¹) than YSZ-based TBC (0.8–2.25 W/mK⁻¹). Moreover, differences between the thermal conductivity values of the GZ and YSZ were higher at higher temperatures (900–1100°C). In different studies [29, 30], Mahade et al. produced single-layered YSZ, double-layered GZ/YSZ, and triple-layered GZ dense/GZ/YSZ TBCs by SPS process. The thickness of the layers was different in the studies. As a result of thermal conductivity measurements, they showed that single-layered YSZ-based TBC had higher thermal conductivity than that of double-layered and triple-layered GZ-based systems. This situation was attributed to both oxygen vacancies in the crystal structure and larger difference between atomic weights of the cations of the GZ-based TBC. In another study [35], single-layered GZ and multilayered GZ/YSZ + Yb₂O₃ + Gd₂O₃ TBCs were produced by EB-PVD process and analyzed their thermal conductivities at temperatures between 25 and

1316°C. They observed slight reduction in the thermal conductivity of the coatings thanks to multilayered design (1.13–1.42 and 1.10–1.22 W/mK⁻¹) for single and multilayered systems, respectively. This decrease was tried to be explained by increasing porosity and hemispherical reflection of the multilayered design. In the case of sintering (fully dense material), GZ had lower thermal conductivity than YSZ (1.6–2.3 W/mK⁻¹ at 700°C for GZ and YSZ, respectively) due to the higher concentration of oxygen vacancies of GZ and atomic weight difference between Gd and ZrO₂ [17]. These oxygen vacancies and atomic weight differences gave rise to an effective phonon scattering.

3.2 Mechanical properties of gadolinium zirconate-based thermal barrier coatings

Table 2 shows some of the mechanical properties of YSZ- and GZ-based TBCs produced by APS and sintering techniques. The bonding strength of a coating to a substrate or cohesion strength of the coating has been determined by using adhesion test. This test has been carried out according to the ASTM C-633 standard test method. The bonding strengths of GZ/CYSZ multilayered and functionally graded TBCs that were produced by APS were determined by using ASTM C-633 test method [8]. The bonding strength values of the single-layered GZ and Mled and FGed GZ/CYSZ TBCs having 2, 4, 8, and 12 layers changed between 8.87 and 12.1 MPa. This changing in the bonding strength was attributed to the changing porosity level of the coatings. As the porosity value increased, the adhesion strength of the coating decreased. On the other hand, bonding strength values of the GZ-based TBCs (8.87–12.1 MPa) were comparable to single-layered YSZ-based TBC (10.1 MPa) produced by the same technique [37]. Fracture type of the single-layered GZ coating was fully adhesive (fracture at the bond coat/ceramic top coat interface), but complex adhesive/cohesive fracture was seen (fracture both bond coat/ceramic top coat interface and within the ceramic top coat layers) in the Mled and FGed coatings. No fracture was observed at the bond coat/substrate interface.

Carpio et al. [23] analyzed the hardness of double-layered and functionally graded GZ/YSZ TBCs produced by APS. The hardness values of the TBCs were 4.0 and 4.1 for double-layered and functionally graded GZ/YSZ, respectively. On the

Design	Composition	Production technique	Bonding strength (MPa)	Hardness (GPa)	Elasticity modulus (GPa)	Reference
Single layered	GZ	APS	12.10	—	—	[8]
Multilayered	GZ/CYSZ		8.87–10.18			
Functionally graded			9.21–10.68			
Double layered	GZ/YSZ	APS	—	4.0	—	[23]
Functionally graded				4.1		
Single layered	YSZ	APS	10.1	—	—	[37]
Fully dense	GZ	Sintering	—	10.0	205	[17]
Fully dense	GZ	Sintering	—	6.0	215	[3]

Table 2. Mechanical properties of GZ- and YSZ-based materials produced via different processes and having different designs.

other hand, hardness value of the sintered (fully dense) GZ was changing between 6.0 and 10.0 GPa [3, 17]. The reason of this increase in the hardness was related with the reduction of porosity and cracks after sintering process. It is suggested to investigate the mechanical properties of the GZ-based TBCs produced by EB-PVD technique in future works.

3.3 Thermal cycling and thermal shock performance of gadolinium zirconate-based thermal barrier coatings

Thermal cycling performance test has been generally conducted by heating the TBCs to the exact temperatures in exact time, holding them at that temperature in exact time and cooling them to a certain temperature. Therefore, the failure mechanism in the TBC that is exposed to the thermal cycle test is associated with the stress produced by growth and shrinkage of TGO during heating and cooling. As a result, complex failure morphologies such as cracks propagating within the TBC, at TBC/TGO and TGO/bond coat interface, come into existence. On the other hand, thermal shock test has been carried out by sudden heating and cooling of the TBCs. Thermal shock resistance of the TBC material depends on the its thermal expansion coefficient, elastic module, fracture resistance, and phase transformation phenomenon.

As already mentioned before (introduction part), GZ has very advantageous properties (low thermal conductivity, high phase stability and higher CMAS, and hot corrosion resistance than YSZ) as TBC material, but its thermal cycle and thermal shock performance is poor. Therefore, works on GZ-based TBC are focused on improving its thermal cycling and thermal shock performance. Thermal cycling performance of the MLed and FGed GZ/CYSZ TBCs was tested by using gas burner method (oxy-propane flame) [8]. TBCs were heated to 1250°C for 1 min and cooled below 150°C by using air jet. According to the results, single-layered GZ fully spalled after 165 cycles, and there was a small edge spallation in the MLed GZ/CYSZ TBCs after 300 cycles. However, there was no visible spallation in the FGed GZ/CYSZ TBCs even after 300 cycles. The microstructural characterizations of MLed and FGed GZ/CYSZ TBCs after thermal cycling test revealed that TGO layer played an active role on the spallation of single-layered GZ. In the case of MLed GZ/CYSZ TBCs, horizontal cracks propagating inside the ceramic coating layers were observed. On the other hand, there was no microcrack or spallation in the FGed GZ/CYSZ TBCs. It was concluded that an improvement in the thermal cycling performance of the single-layered GZ TBC took place thanks to MLed and FGed designs. Furthermore, GZ/CYSZ TBCs having FGed design had superior thermal cycling performance than that of MLed design. As a continuation of the previous work, in another study [14], these TBCs (MLed and FGed GZ/CYSZ coatings) were subjected to the thermal shock test. During the test, the TBCs were directly placed to the furnace at 1250°C and hold for 5 min. Then they were dropped into the cold water. As seen in **Figure 7**, single-layered GZ and YSZ (sample codes: GZ1 and YSZ1, respectively) TBCs were subjected to the thermal shock test as reference samples as well as MLed and FGed TBCs, and the number of cycles to failure for each coating was written on the images. The failure or spallation took place on the coating of single-layered GZ1 after only ten cycles. On the other hand, a significant improvement happened in the thermal shock lifetime of the MLed and FGed TBCs.

This improvement in thermal shock lifetime of TBCs having MLed and FGed designs was ascribed to the decreasing high thermal mismatch stress generated due to the sharp differences in the CTE between bonding layer and CYSZ and GZ phases. As mentioned before CYSZ had higher CTE ($13 \times 10^{-6} \text{ K}^{-1}$) than GZ ($10.4 \times 10^{-6} \text{ K}^{-1}$). Therefore, large thermal expansion mismatch among ceramic

layers, metallic bond coat, and substrate was balanced thanks to gradual compositional variation of CYSZ layers having in GZ layers. Furthermore, microstructural evaluations were carried out on GZ/CYSZ MLED and FGed TBCs exposed to thermal shock test. Microstructures of the GZ-based TBCs after thermal test showed the evidence of the thermal stress on the ceramic layer. The vertical, horizontal, and propagating cracks were formed on the ceramic top layers. Propagating cracks are located around the vertical cracks. The shape of the vertical cracks was looking like capillary vessels. Other than this, there were penetrating cracks forming in the TGO layer and penetrating into the bond coat. A similar microstructure regarding the shape of the cracks of thermally cycled TBCs was reported in other studies [23, 38]. As a result, the improvement in thermal shock life of GZ-based TBCs was directly reducing the thermal mismatch among the layers thanks to CYSZ. Furthermore, from the microstructures, it was assumed that energy of thermal fatigue cracks absorbed at the interface between GZ and CYSZ layers or splats causing improvement in thermal shock life.

In a study [22], double-layered GZ/YSZ TBCs were produced by APS technique so as to have different porosity values. Then thermal cycling behavior of the TBCs were tested at 1400°C by using a gas flame (for heating) and air jet (for cooling). Results showed that thermal cycling lifetime of the single-layered GZ was significantly improved thanks to a double-layered design. Moreover, GZ/YSZ TBCs having the highest porosity level (%32) withstood up to 1627 thermal cycles. Carpio et al.

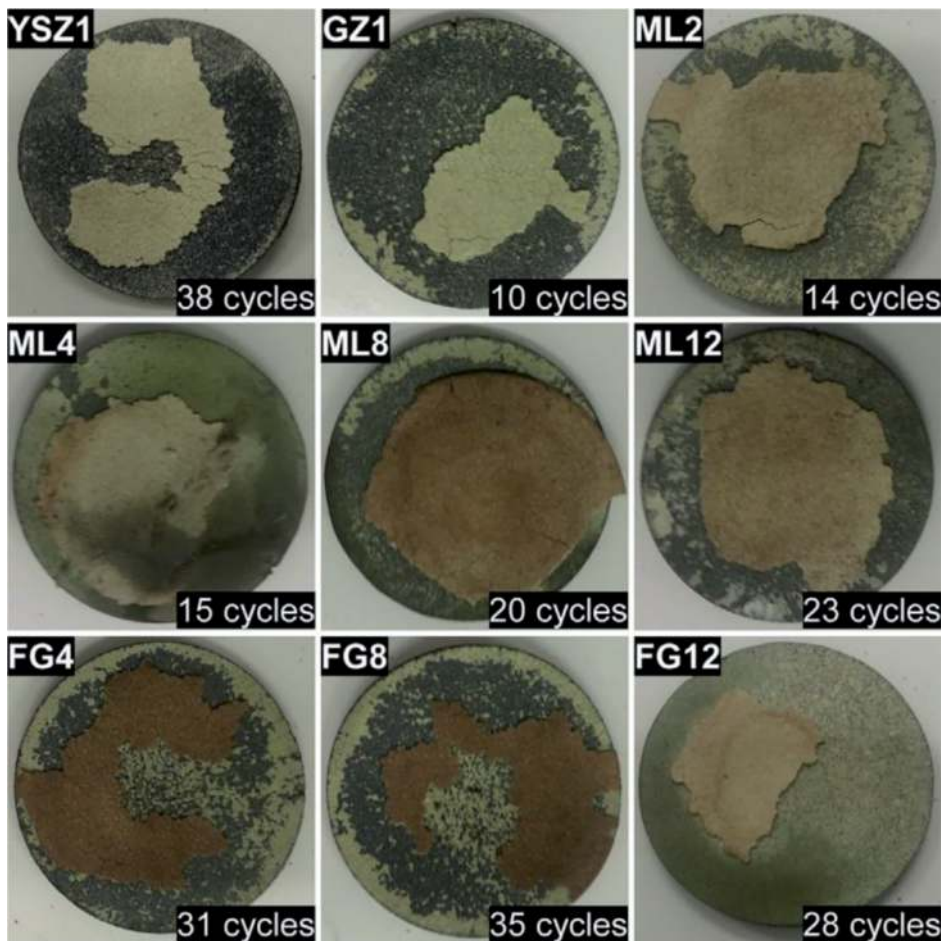


Figure 7. Macroscopic image showing remaining top coats on the substrate after thermal shock test and number of cycles to failure.

produced MLED and FGed GZ/YSZ TBCs by APS technique [23]. The GZ/YSZ TBCs having two and five layers were exposed to thermal cycling test in the furnace. The TBCs were heated to 1050°C and then cooled by air. The thermal cycling life of the MLED GZ/YSZ TBC was about 1000 cycles. On the other hand, FGed GZ/YSZ TBC had resistance up to about 2300 cycles. This situation was attributed to the homogenous distribution of thermal stress in the layers of FGed coating. Mahade et al. subjected the specimens of double- and triple-layered (GZ dense/GZ/YSZ) TBCs that were produced by SPS technique to the thermal cycling test. The thermal cycling tests were carried out in the furnace (heating the specimens up to 1100 and 1200°C for 1 hour and cooling to 100°C). Researchers concluded that an improvement in the thermal cycling lifetime took place thanks to GZ dense/GZ/YSZ triple-layer approach. This was due to the lower porosity content of triple-layer approach. Thanks to dense GZ layer, less oxygen has reached to the bond layer. As a result, the thickness of TGO had remained below the critical value causing failure in the coating. In another study by Zhang et al. [6], double-layered Yb₂O₃-doped GZ (GYbZ)/YSZ TBCs are produced by EB-PVD technique. They produced two sets of (GYbZ)/YSZ TBCs. One of them had normal (sharp) interface between GYbZ and YSZ phases. On the other hand, another set of the TBCs had a uniform interface with a fluent transition (gradient coating) region (nearly 10 μm). Results of thermal cycling test, which was carried out by heating the surface of the TBCs up to 1350°C by a flame and cooling by compressed air, showed that TBC having a gradient transition region had higher lifetime (1346 cycles) than that of TBC having sharp interface (942 cycles). This beneficial effect of the gradient transition region was attributed to the gradually compositional change reducing the thermal mismatch at the interface between ceramic layers.

Consequently, it is possible to prolong the thermal cycling and thermal shock lifetime of the GZ by using a second material (such as YSZ and CYSZ) in multilayered and functionally graded designs. The stress generated by thermal mismatch has been reduced and reaction tendency of the GZ with TGO layer prevented thanks to multilayered and functionally graded designs.

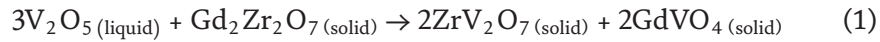
4. Attack of harmful foreign substances

4.1 CMAS and hot corrosion resistance of gadolinium zirconate-based thermal barrier coatings

The jet engine fuel especially used in military aircrafts has low quality, and it contains appreciable levels of impurities such as Na₂SO₄ + V₂O₅. They cause severe damage on the ceramic top layer at high temperatures [14, 26, 39]. On the other hand, calcium-magnesium-alumino-silicate (CMAS) is known as airborne silicate particles (sand, ash, dust, etc.). The CMAS entering to the turbine melts on the hot TBC surfaces and penetrates into the ceramic top coat. This situation leads to premature failure of the coating [12, 14]. There are a lot of studies in the literature proving that GZ-based TBCs have excellent CMAS and hot corrosion resistance.

In the studies that were carried out by Habibi et al. [21, 24], YSZ- and GZ-based TBCs were produced by APS technique. To evaluate hot corrosion behavior of the TBCs, hot corrosion powders (Na₂SO₄ + V₂O₅) were applied (20 mg/cm²) on the TBCs, and they were cyclically exposed to the 1050°C. The failure of the YSZ-based top coat started after 24 hours and spallation occurred. The detailed characterizations revealed that YVO₄-type crystals formed as result of the reactions between yttria (Y₂O₃) and V₂O₅ or NaVO₃. This formation of the YVO₄ caused the transformation of ZrO₂ from tetragonal to monoclinic due to the leaching of the Y₂O₃ from

the YSZ. On the other hand, failure in the GZ-based coating started after 36 hours. This situation showed that GZ-based coating had much better hot corrosion resistance than that of YSZ. In the case of GZ-based coating, molten $\text{Na}_2\text{SO}_4 + \text{V}_2\text{O}_5$ mixture reacts with the bulk $\text{Gd}_2\text{Zr}_2\text{O}_7$ layer to form GdVO_4 . However, $\text{Na}_2\text{SO}_4 + \text{V}_2\text{O}_5$ mixture attacks to the Y_2O_3 that is stabilizer of YSZ. Liu et al. [26] investigating hot corrosion behavior of sintered GZ in the presence of V_2O_5 explained the reaction mechanism. According to this, at 700°C molten V_2O_5 started to react with $\text{Gd}_2\text{Zr}_2\text{O}_7$ to form ZrV_2O_7 and GdVO_4 (see Eq. (1)). In the case of $750\text{--}850^\circ\text{C}$, the final reaction products of GdVO_4 and $m\text{-ZrO}_2$ formed depleting V_2O_5 (see Eq. (2)):



Suspension plasma-sprayed (SPSed) GZ/YSZ TBCs having multilayered designs were subjected to the hot corrosion test [25]. V_2O_5 and Na_2SO_4 salts were applied to the specimen surface at a concentration of 4 mg/cm^2 . The test was conducted at 900°C for 8 hours. Microstructures revealed that GZ-based coatings had lower reactivity with the corrosive salts and the formation of gadolinium vanadate (GdVO_4).

Another promising feature of the GZ is its high resistance to CMAS attack. In contrast to conventional YSZ, GZ is highly effective in resistance to the penetration of molten Ca-Mg-Al-silicate (CMAS) glass deposit. This higher resistance of the APSed GZ-based TBC was proven for prolonged durations [40]. The CMAS sand was applied to the surface of the TBCs at a concentration of 35 mg/cm^2 . Then TBCs were heated to 1200°C in air for 24 and 168 hours in a furnace. Results showed that CMAS melt was fully penetrated inside of the YSZ. The penetration depth of YSZ-based TBC was approximately $200 \mu\text{m}$. However, CMAS melt was arrested on the surface of GZ-based coating (at a penetration depth $20 \mu\text{m}$). This resistance of the GZ-based TBC was attributed to the formation of a crystalline sealing layer. The chemical composition of the sealing layer was $\text{Ca}_2\text{Gd}_8(\text{SiO}_4)_6\text{O}_2$ (apatite phase), and it formed as a result of the high-temperature chemical interactions between the GZ and CMAS melt. Similar results were found for GZ-based TBC that was produced by EB-PVD technique [20]. The mechanism of the CMAS resistance of GZ-based TBC was explained via formation of a highly stable apatite phase. This phase sealed the flow channels of GZ-based SPSed TBC.

In a unique study [14], GZ- and YSZ-based TBCs were produced by APS technique, and they were exposed to CMAS and hot corrosion (CMAS + hot corrosion) test. This test was executed in the same experiment at once. Moreover, a defocused CO_2 laser beam was used as heat source, and TBCs were simultaneously cooled from the back surface of the substrate to create a thermal gradient and harsh environment. Hot corrosion and CMAS powders were applied on the surface of the TBCs together at a concentration of 30 mg/cm^2 , and they were heated by a laser beam to 1250°C and held at that temperature for 1 hour. The rodlike structures formed on both YSZ- and GZ-based coatings. The chemical composition of the rodlike structures was in the form of YVO_4 and GdVO_4 for YSZ and GZ, respectively. The micrographs of the YSZ-based TBC clearly demonstrate that CMAS + hot corrosion products penetrated through microcracks and pores. However, there was a continuous reaction layer formed at the boundary between CMAS and GZ-based TBC. The thickness of reaction layer was approximately $6 \mu\text{m}$. The lamellar microstructural morphology of APSed TBCs turned into a denser structure seeming to extend crystals into the CMAS. This situation was consistent with the similar studies that investigated interactions between GZ-based TBCs and different CMAS sands [20, 23, 40].

Further penetration of the CMAS products into the GZ based was prevented thanks to this reaction (sealing) layer. The formation and sealing mechanism of the reaction layer were defined as follows:

1. The GZ grains were wetted by CMAS melt at the high temperatures.
2. Gd unified with the glass locally.
3. The crystallization initiated in the Gd-rich region of the glass.
4. The apatite ($\text{Ca}_2\text{Gd}_8(\text{SiO}_4)_6\text{O}_2$) and small amounts of other phases formed after crystallization in the Gd-rich region of the glass.
5. The apatite phase prevented further penetration of the molten CMAS glass into the TBC providing a sealing layer between TBC and CMAS.

Gledhill et al. [2] applied the lignite fly ash on the surface of APSed YSZ- and GZ-based TBCs at 1200°C. They showed that the molten lignite fly ash completely penetrated (throughout entire thickness) inside the YSZ-based TBC. Unlike this, the molten lignite fly penetrated only approximately 25% of the GZ-based TBC thickness thanks to a crystalline reaction layer arresting molten fly ash on the TBC.

5. Laser surface modification

5.1 Laser surface modification of gadolinium zirconate-based thermal barrier coatings

Surface modification by using laser beam is a new and good technique for improving some of the properties of plasma-sprayed TBCs. According to the studies, laser remelting solidification process has provided a reduction in the surface roughness and specific surface area. Moreover, besides a columnar cross-sectional structure, controlled (varied depending on the laser parameters) segmented crack network that is perpendicular to the surface can be achieved with sealed porosities at the surface of the coatings. Therefore, hardness, thermal cycle lifetime, resistance to hot corrosion, CMAS, and erosion property of TBCs can be further improved by laser surface modification [1, 7, 11, 13, 18, 41–43]. After laser surface-modified process:

1. Erosion, CMAS, and hot corrosion resistance of the TBC can be enhanced owing to reduction in the surface roughness and specific surface area as well.
2. Thermal shock resistance of the TBC can be enhanced due to segment cracks generated on the surface of the TBC.
3. Thermal cycle lifetime of the TBC can be increased thanks to segmented cracks improving strain accommodation capability.
4. Hardness of the TBC can be increased by changing grain size.

After laser surface modification, a TBC surface should:

1. Have a remelted layer having melting depth of 20–50 μm .

2. Be nonseparated from the as-sprayed layer.
3. Have a smooth surface (with surface roughness value (R_a) lower than $5 \mu\text{m}$).
4. Have a distribution of the crack network that is equiaxed.

All of these properties can be obtained only at optimum laser surface modification parameters. A study of the laser surface modification was made to determine the optimum laser surface modification parameters of APSed GZ-based TBC [13]. The GZ-based TBCs were subjected to the laser surface modification process by using a continuous CO_2 laser. Laser parameters were laser power density on the surface, scanning speed, and laser distance (distance to the surface from the laser torch). During studies, single laser beam tracks were generated on the specimens, and they were examined. As seen in **Figure 8a**, a very successful laser-glazed surface of GZ-based TBC was obtained having a denser microstructure than as-sprayed layer with an average thickness of molten layer $\sim 37 \mu\text{m}$, and a smooth surface (R_a : $2.9 \mu\text{m}$) was accomplished at the optimum laser parameters (laser power density, 70 MW/m^2 ; scanning speed, 150 mm/sn ; laser distance, 14 mm). There was no separation from the as-sprayed layer. Furthermore, the network of cracks were very regular and excellent. These changes in the microstructure of the GZ-based TBC can be clearly noticed in **Figure 8a** when it is compared with **Figure 3a** belonging to the as-sprayed GZ-based TBC surface. **Figure 8b** shows high magnification microstructure of the fracture surface of GZ-based TBC. Individually, glazed layer and as-sprayed structure can be seen clearly. Characteristic cross-sectional microstructure of APSed TBC having splats, parallel cracks at splat boundaries, and pores transformed to dense and nonporous structure at the laser surface-modified layer. During the laser surface modification

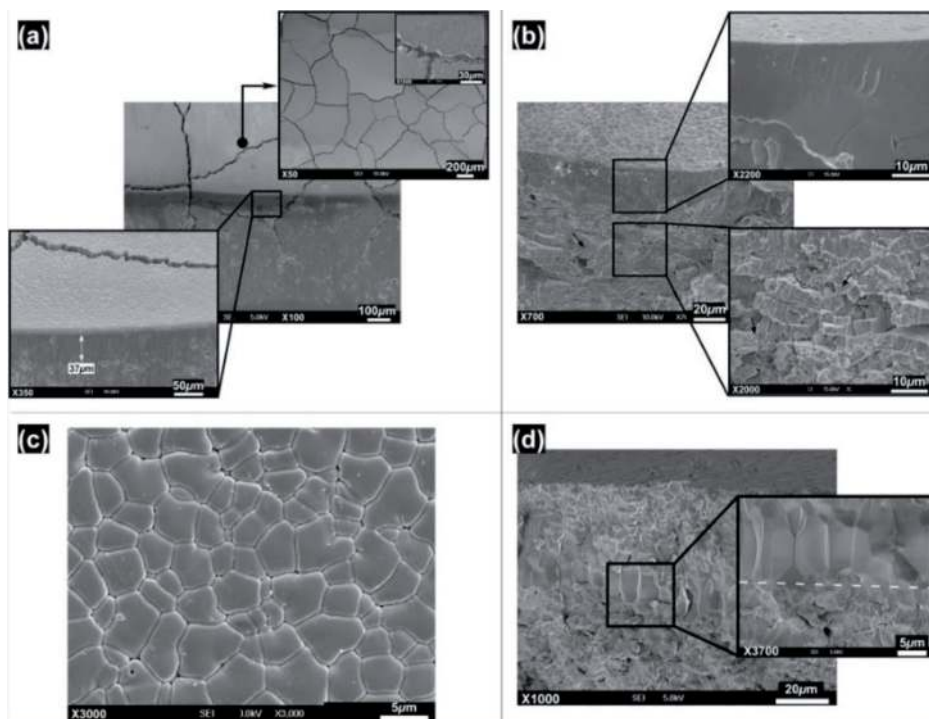


Figure 8. (a) Surface and cross-sectional micrograph of the GZ-based TBC after laser surface modification process, (b) cross-sectional fracture surface micrograph of the GZ-based TBC after laser surface modification process, (c) grain size distribution of the laser surface-modified GZ-based TBC, (d) cross-sectional fracture surface micrograph of the laser surface-modified GZ-based TBC showing columnar grains.

process, molten liquid GZ is replaced with microholes due to the surface tension force of liquid material. On the other hand, laser surface modification parameters affected the grain size and morphology of the GZ-based TBC due to directional solidification. At the optimum laser surface modification parameters (in terms of melting depth, cross-sectional damage, surface quality, and crack network regularity), distribution of the grain size was almost the same, and grains were equiaxed in the GZ-based TBC (see **Figure 8c**). Moreover, as seen in **Figure 8d**, these grains grew as perpendicular to the surface in the laser surface-modified layer of the GZ-based TBC. The structural change from the porous and lamellar plasma-sprayed structure to the columnar laser surface-modified structure could clearly be seen in **Figure 8d**. This structure was due to the directional solidification of laser-modified layer because the direction of heat flow was from the coating to the surface during solidification. This phenomenon was proved by phase analysis. XRD graphs showed that a preferred orientation on the direction took place after laser surface modification process of the GZ-based TBC. On the other hand, hardness value of the remelted regions was affected from the laser surface modification parameters because the grain size of the modified layer decreased as the parameters approach the optimum. The hardness value of laser-glazed GZ-based TBC increased from 10.66 to 12.73 GPa with decreasing grain size. The estimated cooling rate of the remelted layer of GZ-based TBC was about 10^3 – 10^4 °C s⁻¹.

6. Conclusion

In the present chapter, the potential utilization of gadolinium zirconate (GZ) for thermal barrier coating (TBC) applications had been discussed. The production methods, design process, thermal and mechanical properties, failure mechanism, CMAS and hot corrosion resistance, and laser surface modification process of GZ-based TBCs were evaluated in this chapter.

A variety of coating techniques such as atmospheric plasma spraying (APS), solution plasma spraying (SPS), and electron beam-physical vapor deposition (EB-PVD) exist for the production of GZ-based TBCs. The production technique has a significant influence both on microstructure and properties of the GZ-based TBCs. APS is an effective technique to achieve characteristic TBC structure. Thermal conductivity value of the GZ-based TBCs is lower than that of yttria-stabilized zirconia (YSZ). It is possible to further improve the thermal conductivity and thermal failure properties of the GZ-based TBCs by using different coating architectures such as multilayer and functionally graded designs. GZ-based TBCs have a significant advantage in terms of its CMAS and hot corrosion resistance. After laser surface modification of GZ-based TBC, a thin, dense, and smooth remelted layer can be acquired. Furthermore, an equiaxed continuous segmented crack network forms on the surface of laser surface-modified GZ-based TBC. As a result, it was concluded that GZ is an important and promising alternative TBC material.

7. Suggestions

In the future works:

1. New strategies should be introduced to further increase the thermal cycling performance and thermal shock lifetime of the GZ-based TBCs.
2. Mechanical properties of the GZ-based TBCs produced by EB-PVD and SPS techniques should be investigated.

3. Changes in the bonding strength, thermal conductivity, thermal cycling behavior, CMAS, and hot corrosion resistance properties of the GZ-based TBCs after laser surface modification should be examined.
4. In the experiments used to determine the thermal properties of the GZ-based TBCs, new scenario and/or more harsh conditions that are close to the actual operating conditions of the turbine engine should be created.

Acknowledgements

The authors thank Prof. Dr. Yilmaz Taptik, Prof. Dr. Ozgul Keles, Assist. Prof. Dr. Nuri Solak, and Hasan Huseyin Sezer for their contributions.

Author details


Mustafa Guven Gok¹ and Gultekin Goller^{2*}

1 Department of Materials Science and Engineering, Hakkari University, Hakkari, Turkey

2 Department of Metallurgical and Materials Engineering, Istanbul Technical University, Istanbul, Turkey

*Address all correspondence to: goller@itu.edu.tr

IntechOpen

© 2019 The Author(s). Licensee IntechOpen. This chapter is distributed under the terms of the Creative Commons Attribution License (<http://creativecommons.org/licenses/by/3.0>), which permits unrestricted use, distribution, and reproduction in any medium, provided the original work is properly cited. 

References

- [1] Ahmadi-Pidani R, Shoja-Razavi R, Mozafarinia R, Jamali H. Improving the thermal shock resistance of plasma sprayed CYSZ thermal barrier coatings by laser surface modification. *Optics and Lasers in Engineering*. 2012;**50**:780-786. DOI: 10.1016/j.optlaseng.2011.12.007
- [2] Gledhill AD, Reddy KM, Drexler JM, Shinoda K, Sampath S, Pature NP. Mitigation of damage from molten fly ash to air-plasma-sprayed thermal barrier coatings. *Materials Science and Engineering A*. 2011;**528**:7214-7221. DOI: 10.1016/j.msea.2011.06.041
- [3] Zhao M, Ren X, Pan W. Mechanical and thermal properties of simultaneously substituted pyrochlore compounds $(\text{Ca}_2\text{Nb}_2\text{O}_7)_x(\text{Gd}_2\text{Zr}_2\text{O}_7)_{1-x}$. *Journal of the European Ceramic Society*. 2015;**35**:1055-1061. DOI: 10.1016/j.jeurceramsoc.2014.10.009
- [4] Singh R, Rauwald KH, Wessel E, Mauer G, Schrufer S, Barth A, et al. Effects of substrate roughness and spray-angle on deposition behavior of cold-sprayed Inconel 718. *Surface and Coatings Technology*. 2017;**319**:249-259. DOI: 10.1016/j.surfcoat.2017.03.072
- [5] Di Ferdinando M, Fossati A, Lavacchi A, Bardi U, Borgioli F, Borri C, et al. Isothermal oxidation resistance comparison between air plasma sprayed, vacuum plasma sprayed and high velocity oxygen fuel sprayed CoNiCrAlY bond coats. *Surface and Coatings Technology*. 2010;**204**:2499-2503. DOI: 10.1016/j.surfcoat.2010.01.031
- [6] Zhang H, Guo L, Ma Y, Peng H, Guo H, Gong S. Thermal cycling behavior of $(\text{Gd}_{0.9}\text{Yb}_{0.1})_2\text{Zr}_2\text{O}_7/8\text{YSZ}$ gradient thermal barrier coatings deposited on Hf-doped NiAl bond coat by EB-PVD. *Surface and Coatings Technology*. 2014;**258**:950-955. DOI: 10.1016/j.surfcoat.2014.07.051
- [7] Akdogan V, Dokur MM, Goller G, Keles O. Surface modification of thermal barrier coatings by single-shot defocused laser treatments. *Journal of Materials Engineering and Performance*. 2013;**22**:2500-2509. DOI: 10.1007/s11665-013-0548-5
- [8] Guven Gok M, Goller G. Production and characterisation of GZ/ CYSZ alternative thermal barrier coatings with multilayered and functionally graded designs. *Journal of the European Ceramic Society*. 2015;**36**:1755-1764. DOI: 10.1016/j.jeurceramsoc.2016.01.036
- [9] Mahade S, Curry N, Bj S, Orklund € , Markocsan N, En N. Failure analysis of $\text{Gd}_2\text{Zr}_2\text{O}_7/\text{YSZ}$ multi-layered thermal barrier coatings subjected to thermal cyclic fatigue. 2016;**689**:2-10. DOI: 10.1016/j.jallcom.2016.07.333
- [10] Mauer G, Jarligo MO, Mack DE, Vaßen R. Plasma-sprayed thermal barrier coatings: New materials, processing issues, and solutions. *Journal of Thermal Spray Technology*. 2013;**22**:646-658. DOI: 10.1007/s11666-013-9889-8
- [11] Park JH, Kim JS, Lee KH, Song YS, Kang MC. Effects of the laser treatment and thermal oxidation behavior of CoNiCrAlY/ZrO₂₋₈ wt%Y₂O₃ thermal barrier coating. *Journal of Materials Processing Technology*. 2008;**201**:331-335. DOI: 10.1016/j.jmatprotec.2007.11.192
- [12] Senturk BS, Garces HF, Ortiz AL, Dwivedi G, Sampath S, Pature NP. CMAS-resistant plasma sprayed thermal barrier coatings based on Y₂O₃-stabilized ZrO₂ with Al³⁺ and Ti⁴⁺ solute additions. *Journal of Thermal Spray Technology*. 2014;**23**:708-715. DOI: 10.1007/s11666-014-0077-2
- [13] Gok MG, Goller G. Microstructural evaluation of laser remelted gadolinium

zirconate thermal barrier coatings. *Surface and Coatings Technology*. 2015;276:202-209. DOI: 10.1016/j.surfcoat.2015.06.074

[14] Gok MG, Goller G. Microstructural characterization of GZ/CYSZ thermal barrier coatings after thermal shock and CMAS + hot corrosion test. *Journal of the European Ceramic Society*. 2017;37(6):2501-2508. ISSN 0955-2219. <https://doi.org/10.1016/j.jeurceramsoc.2017.02.004>

[15] Cao XQ, Vassen R, Stoeber D. Ceramic materials for thermal barrier coatings. *Journal of the European Ceramic Society*. 2004;24:1-10. DOI: 10.1016/S0955-2219(03)00129-8

[16] Stover D, Pracht G, Lehmann H, Dietrich M, Doring J-E, Vaben R. New material concepts for the next generation of plasma-sprayed thermal barrier coatings. *Journal of Thermal Spray Technology*. 2004;13:76-83. DOI: 10.1361/10599630418176

[17] Wu J, Wei X, Padture NP, Klemens PG, Gell M, García E, et al. Low-thermal-conductivity rare-earth zirconates for potential thermal-barrier-coating applications. *Journal of the American Ceramic Society*. 2002;85:3031-3035. DOI: 10.1111/j.1151-2916.2002.tb00574.x

[18] Ahmadi-Pidani R, Shoja-Razavi R, Mozafarinia R, Jamali H. Laser surface modification of plasma sprayed CYSZ thermal barrier coatings. *Ceramics International*. 2013;39:2473-2480. DOI: 10.1016/j.ceramint.2012.09.005

[19] Mensah PF, Diwan R, Nandikolla S, Coker O, Sahoo P. Thermo-mechanical study of the role of Gd₂Zr₂O₇ (GZ) in improving life of YSZ and GZ double layered thermal barrier coatings (ASME). In: *Proceedings of the International Mechanical Engineering Congress and Exposition*. 2012;88279:3083-3088. DOI: 10.1115/IMECE2012-88279

[20] Kramer S, Yang J, Levi CG. Infiltration-inhibiting reaction of gadolinium zirconate thermal barrier coatings with CMAS melts. *Journal of the American Ceramic Society*. 2008;91:576-583. DOI: 10.1111/j.1551-2916.2007.02175.x

[21] Habibi MH, Wang L, Guo S. An investigation on hot corrosion resistance of plasma sprayed composite YSZ-Gd₂Zr₂O₇ and Gd₂Zr₂O₇ thermal barrier coatings in simulated turbine environment at 1050°C. In: *Des. Mater. Manuf. Parts A, B, C, ASME 2012 International Mechanical Engineering Congress and Exposition*, Vol. 3; 2012. p. 905. DOI:10.1115/IMECE2012-88435

[22] Bakan E, Mack DE, Mauer G, Vaßen R. Gadolinium zirconate/YSZ thermal barrier coatings: Plasma spraying, microstructure, and thermal cycling behavior. *Journal of the American Ceramic Society*. 2014;97:4045-4051. DOI: 10.1111/jace.13204

[23] Carpio P, Salvador MD, Borrell A, Sánchez E. Thermal behaviour of multilayer and functionally-graded YSZ/Gd₂Zr₂O₇ coatings. *Ceramics International*. 2016;43(5):4048-4054. ISSN: 0272-8842. <https://doi.org/10.1016/j.ceramint.2016.11.178>

[24] Habibi MH, Wang L, Guo SM. Evolution of hot corrosion resistance of YSZ, Gd₂Zr₂O₇, and Gd₂Zr₂O₇ + YSZ composite thermal barrier coatings in Na₂SO₄ + V₂O₅ at 1050°C. *Journal of the European Ceramic Society*. 2012;32:1635-1642. DOI: 10.1016/j.jeurceramsoc.2012.01.006

[25] Jonnalagadda KP, Mahade S, Curry N, et al. Hot corrosion mechanism in multi-layer suspension plasma sprayed Gd₂Zr₂O₇/YSZ thermal barrier coatings in the presence of V₂O₅ + Na₂SO₄. *Journal of Thermal Spray Technology*. 2017;26:140-149. <https://doi.org/10.1007/s11666-016-0486-5>

- [26] Liu Z, Ouyang J, Zhou Y, Xia X. Hot corrosion behavior of V_2O_5 -coated $Gd_2Zr_2O_7$ ceramic in air at 700–850°C. *Journal of the European Ceramic Society*. 2009;**29**:2423–2427. DOI: 10.1016/j.jeurceramsoc.2009.01.001
- [27] Ma L, Ma W, Sun X, Ji L, Liu J, Hang K. Microstructures and mechanical properties of $Gd_2Zr_2O_7/ZrO_2(3Y)$ ceramics. *Journal of Alloys and Compounds*. 2015;**644**:416–422. DOI: 10.1016/j.jallcom.2015.05.054
- [28] Li M, Guo L, Ye F. Phase structure and thermal conductivities of Er_2O_3 stabilized ZrO_2 toughened $Gd_2Zr_2O_7$ ceramics for thermal barrier coatings. *Ceramics International*. 2016;**42**:16584–16588. DOI: 10.1016/j.ceramint.2016.07.079
- [29] Mahade S, Curry N, Björklund S, Markocsan N, Nylén P. Thermal conductivity and thermal cyclic fatigue of multilayered $Gd_2Zr_2O_7/YSZ$ thermal barrier coatings processed by suspension plasma spray. *Surface and Coatings Technology*. 2015;**283**:329–336. DOI: 10.1016/j.surfcoat.2015.11.009
- [30] Jonnalagadda KP, Mahade S, Curry N, et al. Hot corrosion mechanism in multi-layer suspension plasma sprayed $Gd_2Zr_2O_7/YSZ$. Thermal Barrier Coatings in the Presence of $V_2O_5 + Na_2SO_4$. *Journal of Thermal Spray Technology*. 2017;**26**:140–149. <https://doi.org/10.1007/s11666-016-0486-5>
- [31] Moskal G, Swadzba L, Hetmanczyk M, Witala B, Mendala B, Mendala J, et al. Characterization of microstructure and thermal properties of $Gd_2Zr_2O_7$ -type thermal barrier coating. *Journal of the European Ceramic Society*. 2012;**32**:2025–2034. DOI: 10.1016/j.jeurceramsoc.2011.11.043
- [32] Wang L, Eldridge JI, Guo SM. Thermal radiation properties of plasma-sprayed $Gd_2Zr_2O_7$ thermal barrier coatings. *Scripta Materialia*. 2013;**69**:674–677. DOI: 10.1016/j.scriptamat.2013.07.026
- [33] Bobzin K, Bagcivan N, Brögelmann T, Yildirim B. Influence of temperature on phase stability and thermal conductivity of single- and double-ceramic-layer EB–PVD TBC top coats consisting of 7YSZ, $Gd_2Zr_2O_7$ and $La_2Zr_2O_7$. *Surface and Coatings Technology*. 2013;**237**:56–64. DOI: 10.1016/j.surfcoat.2013.08.013
- [34] Wessel JK. *The Handbook of Advanced Materials: Enabling New Designs, Functionally Graded Materials*. New Jersey: John Wiley Sons, Inc.; 2004
- [35] Schmitt MP, Rai AK, Bhattacharya R, Zhu D, Wolfe DE. Multilayer thermal barrier coating (TBC) architectures utilizing rare earth doped YSZ and rare earth pyrochlores. *Surface and Coatings Technology*. 2014;**251**:56–63. DOI: 10.1016/j.surfcoat.2014.03.049
- [36] Kelly MJ, Wolfe DE, Singh J, Eldridge J, Zhu DM, Miller R. Thermal barrier coatings design with increased reflectivity and lower thermal conductivity for high-temperature turbine applications. *International Journal of Applied Ceramic Technology*. 2006;**3**:81–93. DOI: 10.1111/j.1744-7402.2006.02073.x
- [37] Karabaş M, Bal E, Taptık İY. Effect of air plasma spray parameters on the properties of YSZ and CYSZ thermal barrier coatings. *Journal of the Australian Ceramic Society*. 2016;**52**:175–182
- [38] Zhou C, Zhang Q, Li Y. Thermal shock behavior of nanostructured and microstructured thermal barrier coatings on a Fe-based alloy. *Surface and Coatings Technology*. 2013;**217**:70–75. DOI: 10.1016/j.surfcoat.2012.11.074
- [39] Liu ZG, Ouyang JH, Zhou Y, Li S. High-temperature hot corrosion behavior of gadolinium zirconate by vanadium pentoxide and sodium sulfate

in air. Journal of the European Ceramic Society. 2010;**30**:2707-2713. DOI: 10.1016/j.jeurceramsoc.2010.05.002

[40] Drexler JM, Chen C-H, Gledhill AD, Shinoda K, Sampath S, Padture NP. Plasma sprayed gadolinium zirconate thermal barrier coatings that are resistant to damage by molten Ca–Mg–Al–silicate glass. Surface and Coatings Technology. 2012;**206**:3911-3916. DOI: 10.1016/j.surfcoat.2012.03.051

[41] Batista C, Portinha A, Ribeiro RM, Teixeira V, Costa MF, Oliveira CR. Morphological and microstructural characterization of laser-glazed plasma-sprayed thermal barrier coatings. Surface and Coatings Technology. 2006;**200**:2929-2937. DOI: 10.1016/j.surfcoat.2004.10.134

[42] Ghasemi R, Shoja-Razavi R, Mozafarinia R, Jamali H. Laser glazing of plasma-sprayed nanostructured yttria stabilized zirconia thermal barrier coatings. Ceramics International. 2013;**39**:9483-9490. DOI: 10.1016/j.ceramint.2013.05.066

[43] Morks MF, Berndt CC, Durandet Y, Brandt M, Wang J. Microscopic observation of laser glazed yttria-stabilized zirconia coatings. Applied Surface Science. 2010;**256**:6213-6218. DOI: 10.1016/j.apsusc.2010.03.143